Electromagnetic Time-Reversal Imaging of the Remote Aerial Targets

Jianglong Zhu*, Xianzheng Zong, Zaiping Nie
University of Electronic Science and Technology of China
Chengdu, China
Email:623447556@qq.com

Abstract—Based on the electromagnetic time-reversal imaging framework, the algorithm for the application scenario excited by multi-antenna is investigated. The main characteristic of the two radar targets is extracted from their scattering matrix by using the method with decomposition of the time-reversal operator (DORT). Then, with using DORT in the transmission mode, the imaging with different radiation source model are compared. At last, the imaging of remote aerial targets is realized by changing the antenna spacing. The simulation results indicate that the imaging of remote aerial targets is feasible.

Keywords—Time-reversal; imaging; decomposition of the time-reversal operator (DORT); scattering; transmission mode .

I. INTRODUCTION

The time-reversal technology (TR) is originated from acoustics. Basic theories have been developed by Fink and Prada. It is shown that the TR focusing is optimal in the sense that it realizes the spatial-temporal matched filter to the propagation transfer function through inhomogeneous media. In particularly, it is a self-adaptive technique that compensate for any geometrical distortions of the array structure as well as for distortions due to the propagation through inhomogeneous media [1]. TR has the advantages and potential in solving some key problems and overcoming a variety of technical difficulties in the field of detection and imaging [2]. It has attracted much attention, due to its computational simplicity as compared to the maximum-likelihood (ML) approach and its possibility of overcoming the Rayleigh bound on the resolution power of classical direction finding methods [3]. The representative algorithms include DORT and multiple signal classification (MUSIC) [4], [5].

However, there is not any ripe theory for the imaging of remote aerial targets in time reversal technology. The purpose of this paper is to explore the influence factors of the remote aerial targets imaging. TR is based on reciprocity principle, in the following discussion, the medium has been assumed to be lossless. Hypothesizing a source emits radiation that propagates through propagation medium to a set of receiving antennas. The data that arrives early in time at a given receiver implicitly travels a shorter distance than data that arrives later in time. Next, the time-reversal operator is obtained by reversing the received waveforms in time which is equivalent to producing a time-reversed field at the phase-conjugate mirror. Ultimately, the singular value decomposition (SVD) of transmission matrix reflects the essence character of the targets.

II. THE THEORY OF ELECTROMAGNETIC TIME-REVERSAL

Assuming that the channel contains $M \times M$ transceiver antennas and S scattering dots, the frequency domain reflection coefficients is $\tau_i(\omega), i=1,2,\cdots S$. Then the transmission matrix $\overline{K}(\omega)$ can be written as the product of the three part,

(1) The transmission matrix $\overline{G}_t(\omega)$ from transmitting array to every scattering dot.

(2) The scattering matrix $\overline{\tau}(\omega)$ of each scattering dot.

(3) The transmission matrix $\overline{G}_r(\omega)$ from each scattering dot to the receiving array.

$$\overline{K}(\omega) = A_r(\omega)A_t(\omega)\overline{G}_r(\omega)\overline{\tau}(\omega)\overline{G}_t(\omega) \qquad (1)$$

Where $A_t(\omega)$ and $A_r(\omega)$ is the response of the transceiver antenna. Then, the time-reversal operator eigenvalue equation can be written as

$$\overline{T}(\omega)\overline{G}_i^*(\omega) = \overline{K}^*(\omega)\overline{K}(\omega)\overline{G}_i^*(\omega) = |\tau_i(\omega)|^2 [\sum_{m'=1}^{M}|G(r_i,r_{m'},\omega)|^2]^2 \overline{G}_i^*(\omega) \qquad (2)$$

Where $\overline{K}^*(\omega)$ is the transpose conjugate of $\overline{K}(\omega)$, the eigenvalue of the time-reversal operator $\lambda_{m'}$ is

$$\lambda_{m'} = |\tau_i(\omega)|^2 [\sum_{m'=1}^{M}|G(r_i,r_{m'},\omega)|^2]^2 \qquad (3)$$

Eigenvector corresponding to the eigenvalue $v_{m'}$ is

$$v_{m'} = \overline{G}_{im'}^*(\omega). \qquad (4)$$

The transmission matrix $\overline{K}(\omega) = [K_{ij}]$, this is a symmetric $M \times M$ matrix and its element K_{ij} is the signal received at the ith antenna when the signal wave is emitted from the jth antenna and reflected by targets. Consider the wave v ($M \times 1$ matrix) applied to the N elements. The wave propagates and is reflected by targets and received by the N receivers. The received signal is then given by $M \times 1$ matrix $\overline{K}(\omega)v$ where $\overline{K}(\omega)$ is the $M \times M$ multi-static data matrix. This received signal is then time reversed at each terminal giving the next transmitted signal $(\overline{K}(\omega)v)^*$.

This process can continue and if this sequence converges, then except for a constant σ, the transmitted signal $(\overline{K}(\omega)v)^*$ is equal to the original transmitted signal v. Where the constant σ represents the power lost by scattering and diffraction.

$$(\overline{K}(\omega)v)^* = \sigma v. \qquad (5)$$

This can be converted to an eigenvalue equation by multiplying both sides by K^*,

$$\overline{K}^*(\omega)\overline{K}(\omega)v = \lambda v \qquad (6)$$

$$\lambda = \left|\sigma^2\right| = eigenvalue \qquad (7)$$

As shown in Fig. 1, eigenvalue λ is the ratio of the received power to the input power, and the largest eigenvalue represents the largest target giving the largest reflected power.
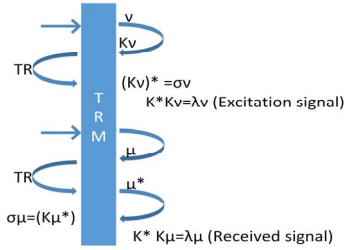

Fig. 1. Excitation signal v is eigenvector of the time-reversal matrix $\overline{T}(\omega)=\overline{K}^*(\omega)\overline{K}(\omega)$. Received signal u is eigenvector of $\overline{T}^*(\omega)$. If the same array is used for excitation and receiver, $u=v^*$.

The signal subspace and the noise subspace based on time-reversal operator can be expressed as

$$\overline{T}(\omega) = (U_S, U_N)\begin{pmatrix}\sum_S & 0 \\ 0 & 0\end{pmatrix}(V_S, V_N)^* \qquad (8)$$

Those eigenvectors with nonzero eigenvalues are said to be in the signal space and the others with zero eigenvalues are in the noise space. It is also shown that the eigenvectors in the signal subspace and in the noise subspace are orthogonal and therefore the inner products of the eigenvectors in the signal subspace and the noise subspace are zero. Noting these, the DORT pseudospectrum can be expressed as

$$P_{DORT}(r) = \sum_{i=1}^{min(M_t, M_r)} \left|<v_i, G_0^*(r)>\right|^2 \qquad (9)$$

Where M_t and M_r is the number of transceiver antennas, v_i is the eigenvector corresponding to the eigenvalue, $G_0^*(r)$ is a free space Green's function. The pseudospectrum then gives a high image peak at the target point.

In practical measurement, because scattering matrix $\overline{S}(\omega)$ is easily measurable, and it implies the main characteristic of the radar targets. In the following discussion, the scattering matrix $\overline{S}(\omega)$ is a substitution for transmission matrix $\overline{K}(\omega)$.
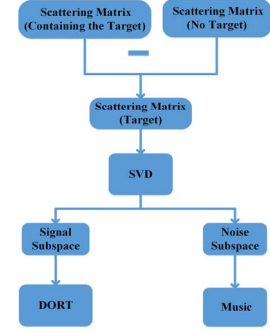

Fig. 2. Imaging process. For computation of each image, two measurements are performed. Firstly, a measurement of the background environment in the absence of the target should be taken, and then a second measurement is performed with the target present. Imaging is performed using the measured data computed by subtracting the first data from the second.

III. TIME-REVERSAL IMAGING

A. Imaging With Different Radiation Source Model

There are two models with different radiation source. The first scenario with dipole radiators is shown in Fig. 3. The working frequency is f_0. The coordinates of the two targets are $(10\lambda, 0\lambda, 6\lambda)$ and $(13\lambda, 5\lambda, 3\lambda)$. The difference is that the radiation source of the second scenario is ideal point source. At last, the DORT algorithm is used for imaging, the result is shown in Fig. 4.
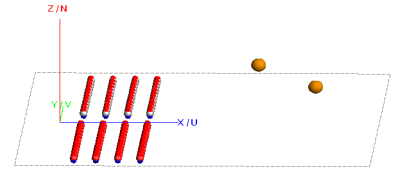

Fig. 3. transmission mode(48×48). The transmitting array antennas(in the minus y direction) and the receiving array antennas(in the y direction) are placed in different positions .They are both composed of 48 elements, each unit is a z-polarized dipole, and the antenna spacing is 2λ in x-direction and y-direction. The two targets on the right are metal balls with a radius of 0.8λ.

As illustrated in the Fig. 4, the two targets are successfully displayed. Although the targets are not far away from the arrays, this work has laid the foundation for the imaging of remote aerial targets. As shown in Fig.5.(b), due to the influence of polarization and structure, the corresponding relation between singular value and targets is much more complex.

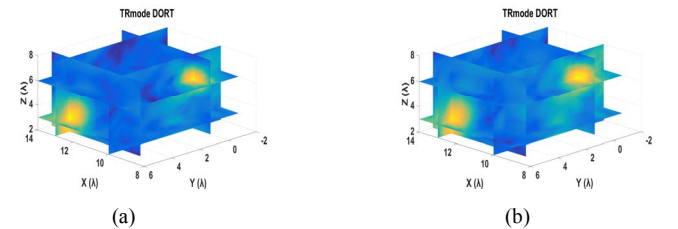(a)   (b)

Fig. 4. (a) Detection imaging based on the transmission matrix of ideal radiation points (48×48). (b) Detection imaging based on the transmission matrix of z-polarized dipoles (48×48).
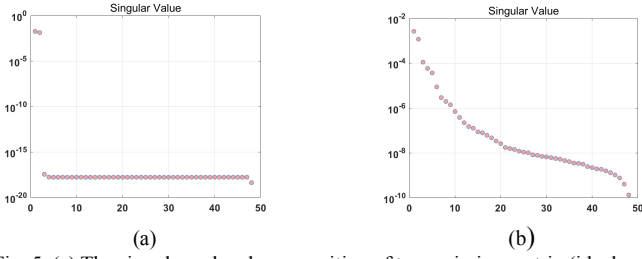
Fig. 5. (a) The singular value decomposition of transmission matrix (ideal point source). (b)The singular value decomposition of transmission matrix (z-polarized dipoles).

B. Imaging of Remote Aerial Targets

Based on the scenario mode shown in Fig. 3, the locations of two targets are changed to $(500\lambda, 0, 506\lambda)$ and $(502\lambda, 0, 509\lambda)$. Regrettably, the imaging shown in Fig. 6.(a) is failing. And the result shown in Fig. 6.(b) gives a effective imaging after increasing the antenna spacing (L) to 40λ, but its imaging result is blurry. Then, the antenna spacing (L) is increased to 80λ, the imaging resolution has been significantly improved due to the increase of array aperture, as shown in Fig.6.(c).
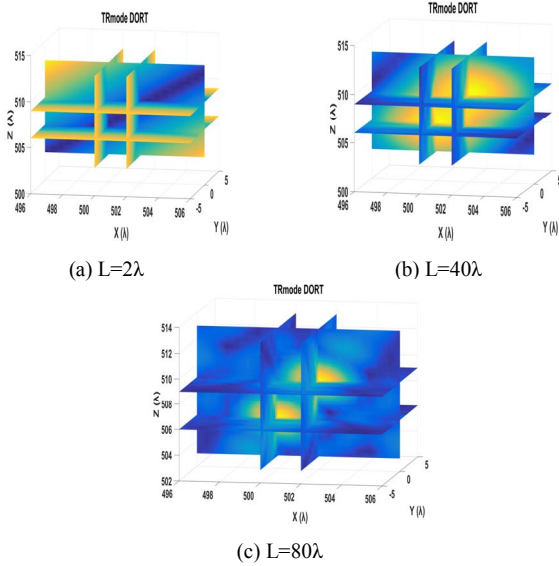

(a) L=2λ

(b) L=40λ

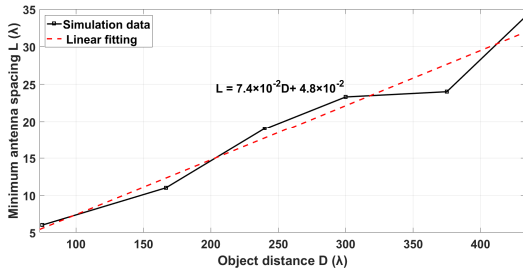(c) L=80λ

Fig. 6. Imaging after increasing the antenna spacing.

Fig. 7. The functional relation between the minimum antenna spacing L and the object distance D, where $D=(x^2+y^2+z^2)^{1/2}$, and (x, y, z) is the coordinates of the further target.

According to the result shown in Fig. 7, the study found a linear relation between the minimum antenna spacing L and object distance D. The further the target, the greater the antenna spacing. Based on the established functional relation, the required antenna spacing can be calculated directly. The imaging of the remote targets is shown in Fig. 8.
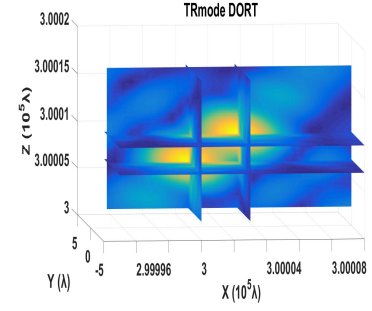

Fig. 8. Imaging of remote targets after fitting the antennas spacing. Where the coordinates of two targets are $(3\times10^5\lambda, 0, 3.00007\times10^5\lambda)$ and $(3.00003\times10^5\lambda, 0, 3.0001\times10^5\lambda)$, the required antenna spacing is $3.1396\times10^5\lambda$.

IV. CONCLUSION

Electromagnetic time-reversal imaging has been verified with decomposition of the time-reversal operator (DORT), and the pseudospectrum gives a high image peak at the targets points. Because the distribution information of the singular value depends on the antennas structure and the state of the targets, how to select the eigenvalues used for the pseudospectrum has a certain influence on the resolution. When the remote targets are imaged, the resolution of imaging can be significantly improved by increasing the antennas spacing within the specifications. Essentially, larger array aperture is achieved that improves the performance of the algorithm effectively. It provides a theoretical basis for the imaging of remote aerial targets by sparse antenna array.

While the imaging results presented here appear encouraging, there are still some problems to be resolved. For example, when the detecting extension is expanded, DORT has the slower calculating speed, and needs more memory. In other words, the imaging has poor real-time performance. And furthermore, the influence of Doppler Effect is also taken into account when the moving objects are imaged.

References

[1] M. Fink, "Time reversal of ultrasonic fields. I. Basic principles," IEEE Trans. Ultrason., Ferroelectr., Freq. Control, vol. 39, no. 5, pp. 555-566, May. 1992.

[2] P. Glotov. "Time Reversal of Electromagnetic Waves in Randomly Layered Media." PhD Dissertation, North Carolina State University, 2006.

[3] P. Stoica and A. Nehorai, "MUSIC, maximum likelihood and Cramer-Rao bound: further results and comparisons," International Conference on Acoustics, Speech and Signal Processing, Glasgow, 1989, vol.4, pp. 2605-2608.

[4] D. H. Chambers and J. G. Berryman, "Analysis of the time-reversal operator for a small spherical scatterer in an electromagnetic field." IEEE Trans. Antennas Propag., vol. 52, pp. 1729-1738, 2004.

[5] J. L. Robert and M. Burcher, "Time reversal operator decomposition with focused transmission and robustness to speckle noise: application to microcalcification detection." Journal of the Acoustical Society of America, vol. 119, no. 6, pp. 3848-3859, 1992.